Acid-Mediated Modulation of the Conductance of Diazapentalene Molecular Junctions

Jianming An,[○] Xiaoqi Luo,[○] Sumit Naskar, Di Wu,* Carmen Herrmann, Jianlong Xia,* and Haixing Li*
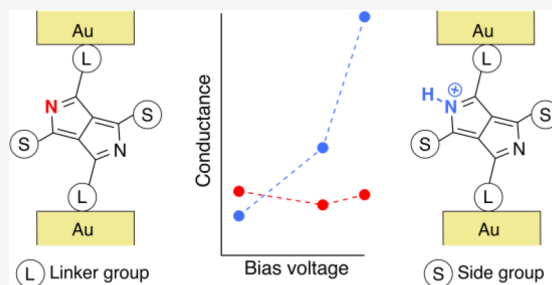
ACCESS | Metrics & More | Article Recommendations | SI Supporting Information

ABSTRACT: We report an acid-mediated regulation of single-molecule junction conductance achieved using an electron-deficient unit, diazapentalene, functionalized with thiophene extending units and thiomethyl aurophilic terminal groups. This diazapentalene derivative exhibits a protonation reaction in the presence of trifluoroacetic acid, as characterized by UV−vis absorption spectroscopy, and the protonated species shows a voltage-dependent single-molecule conductance, which is not observed for the pristine molecules. Specifically, under a high bias voltage of 850 mV, we observe a conductance value for the protonated molecule larger than that for the deprotonated one by a factor of 4. Density functional theory-based transport calculations show a slight broadening of the HOMO and LUMO frontier orbitals, as well as a reduced HOMO−LUMO gap when the molecule becomes protonated; this implies an increased conductance under protonation that is consistent with the experimental conductance data. Our work demonstrates a new molecular design for versatile control of molecular conductance through the use of acid in the solvent environment.

When a molecular-scale device contains molecules that undergo protonation or deprotonation reactions in an acidic or basic environment, the protonation state of the molecule often plays an important role in determining the charge transport properties of the molecular junctions and ultimately the functionalities of the devices. Thus, addition of acid/base into the solvent environment of a single molecule junction becomes an easy and effective means for regulating the junction conductance.[1,2] A range of pH-responsive molecular components, including the commonly used chemical linker groups such as amines and carboxylic acids,[3,4] a less common phenol linker,[5] and backbone components such as imidazoles,[6,7] pyrazoles,[8,9] diketopyrrolopyrrokes,[10] pyridines,[11−13] pyrimidines,[14] spiropyrans,[15,16] azulenes,[17,18] peptides,[19−21] etc.,[22,23] have been used for constructing single-molecule junctions with conductance properties that are regulated by pH. Given the effectiveness of pH as an external control for molecular devices, methods for implementing a pH control and mechanisms underlying the pH-regulated single molecule junction conductance are continuing to be investigated.

In this work, we synthesize a strong electron acceptor diazapentalene flanked by two thiophenes with the terminal thiophenes containing the thiomethyl terminal groups for stable binding to Au electrodes. Protonation reactions at the diazapentalene unit occur in the presence of organic trifluoroacetic acid (TFA), as confirmed by UV−vis spectrometry, and the protonated diazapentalene shows an increased single-molecule conductance compared with that of the deprotonated species. Specifically, we perform conductance

measurements of this diazapentalene compound using the scanning tunneling microscope break-junction (STM-BJ) technique under different bias voltages and show that the protonation reaction at diazapentalene affects the single-molecule junction conductance in a voltage-dependent manner. The protonated compound shows a conductance up to four times that measured for the deprotonated one under a high bias voltage. We further carry out DFT-based transmission calculations; we find that, when the molecule becomes protonated, the frontier molecular orbitals HOMO and LUMO are broadened and HOMO−LUMO peak positions become closer, resulting in larger transmissions at energies between these two frontier orbitals, agreeing with our experimental observation.

We design and synthesize diazapentalene compound **1** following the synthetic procedure as shown in Scheme 1 (details of the synthesis and compound characterization are provided in Supporting Information Parts I, V, and VI). The Stille coupling reaction between compound **2** and **3** afford the compound **1** as a blue solid in 73% yield. The compounds **2** and **3** were synthesized according to the published procedures.[24,25]

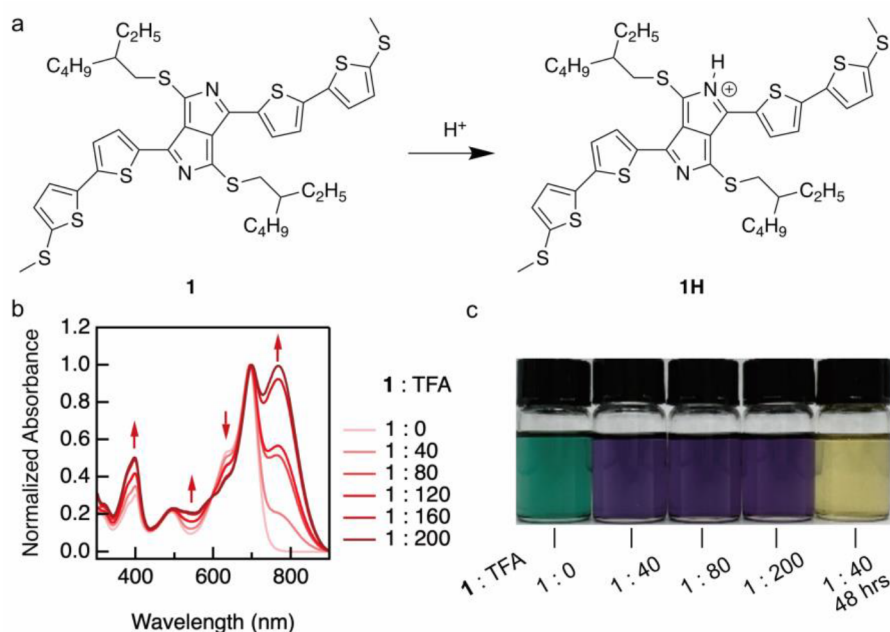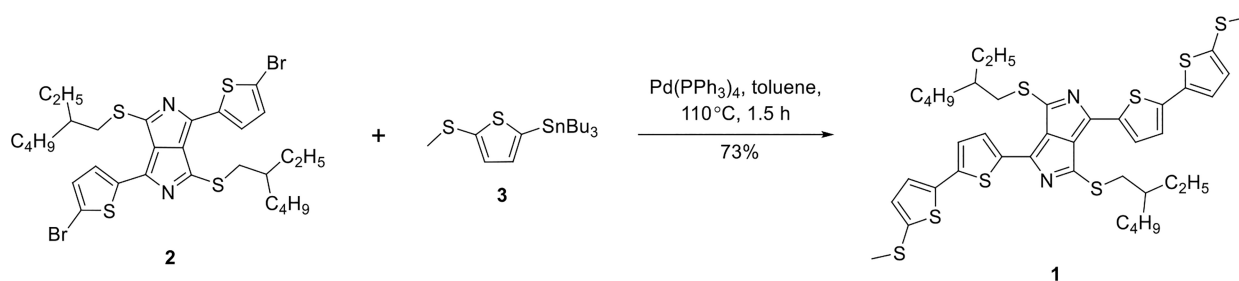**Scheme 1. Synthetic Scheme for Compound 1**

Figure 1. (a) Protonation reaction of compound **1**. (b) Normalized absorption spectra of **1** (normalized at the peak ∼697 nm) in deuterated chloroform with different amounts of trifluoroacetic acid (TFA) added; the concentration ratios between **1** and TFA are listed on the right. (c) Photograph of a solution of 0.002 mM **1** in 1,2,4-trichlorobenzene with different amounts of TFA added. The molar ratio between **1** and TFA is provided at the bottom. All solutions have been freshly made except the one on the right, which was left in air for 48 h prior to the photo being taken.

Previous work on diazapentalene-containing polymers has suggested that a 20-fold excess of TFA was needed for protonating the diazapentalene unit, as TFA (pK_a = 0.2) is considered a weak acid (e.g., for HCl, pK_a = −6.0).[26] To determine the amount of trifluoroacetic acid needed for inducing the protonation reaction of **1** (illustrated in Figure 1a), we performed UV−vis absorption spectroscopy of **1** under a series of acid concentrations. We find that, when **1** is protonated, a new, intense absorption peak at 767 nm appears (Figure 1b). We also observe an increase in absorption at around 397 and 544 nm and a decrease in absorption intensity at around 633 nm, as indicated by the arrows in Figure 1b. These changes in absorption spectra agree well with previous works of other diazapentalene-containing compounds,[24,26,27] indicating the **1** to **1H** reaction. We find that, under lower molar ratios of **1**:TFA of 1:1−1:5, we do not successfully protonate compound **1** as no changes were observed in the absorption spectra (Figure S1), suggesting that an excess amount of acid is needed to protonate the diazapentalene unit when it is connected to an extended backbone structure here. Based on the absorption spectra, we do not reach a saturation limit of protonation in the concentration range tested. We note that, although the diazapentalene unit bears two nitrogen sites

that could undergo a protonation reaction, only one of them is protonated as shown in previous works.[24,26,27] When we prepare a solution of **1** in 1,2,4-trichlorobenzene (TCB) solvent, the color of the solution changes from green to dark purple upon addition of TFA (Figure 1c); the solution with different molar ratios between **1** and TFA will then be used for conductance measurements. We find that, from both color change (Figure 1c, last solution) and absorption spectra, the protonated structure is likely not stable over 48 h or longer; therefore, we use a freshly prepared molecular solution for the charge transport measurements each time (a measurement performed ∼20 days after a molecular solution was prepared is provided in Figure S2).

We next measure the single-molecule conductance of **1** in the absence and presence of organic acid TFA using the STM-BJ technique (experimental details in Supporting Information Part II).[28−30] We use a gold tip and a gold-coated substrate to repeatedly form and rupture gold point contacts in solutions of 0.1 mM **1** in TCB with added TFA at 1:0, 1:40, 1:80, and 1:200 concentration ratios between the target molecule **1** and TFA. Figure 2a−d shows the one-dimensional (1D) conductance histograms of **1** measured under these four different concentrations of added acid. We find that **1** (Figure
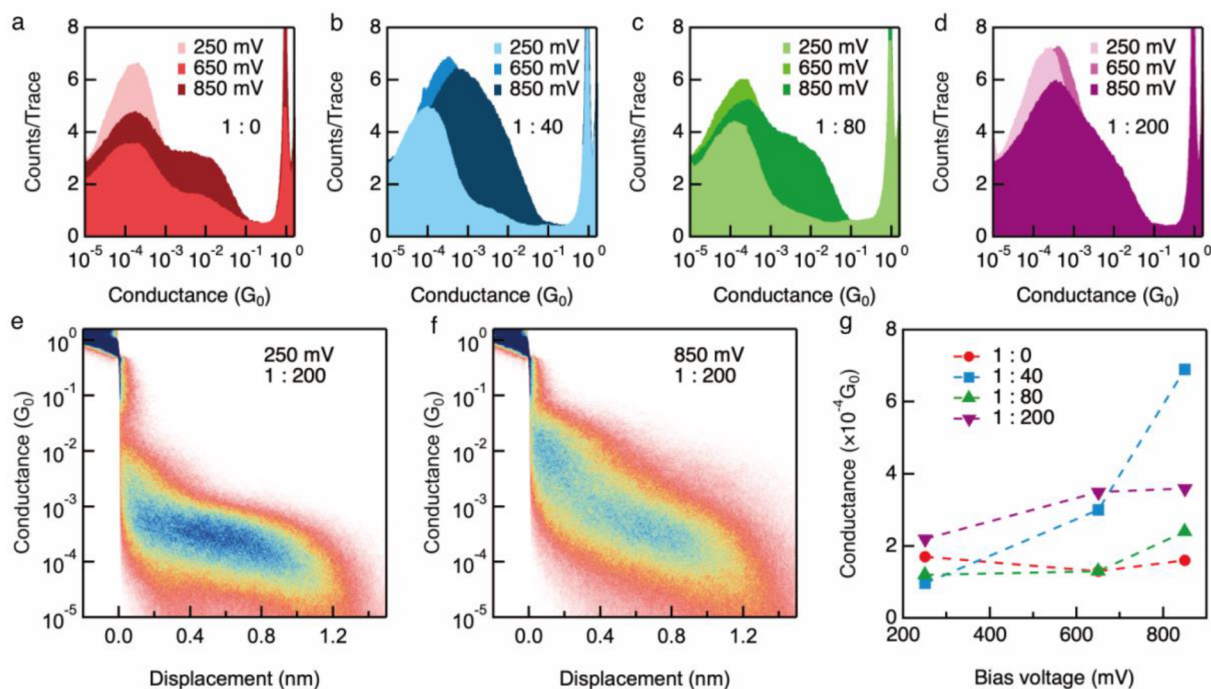
Figure 2. (a–d) Logarithmically binned 1D histograms for **1** measured under a molar ratio between **1** and TFA at (a) 1:0, (b) 1:40, (c) 1:80, and (d) 1:200 under 250 mV, 650 mV, and 850 mV tip bias voltages. (e, f) 2D conductance-displacement histogram for **1** measured at molar ratio **1**:TFA = 1:200 under (e) 250 mV and (f) 850 mV bias voltages. (g) Conductance peak values of the single-molecule junctions for **1** or **1H** at four molar ratios between **1** and TFA of 1:0 (red), 1:40 (blue), 1:80 (green), and 1:200 (purple), respectively, as functions of applied tip bias voltage.

2a) and the protonated **1H** (Figure 2b–d) both form single-molecule junctions with Au electrodes and show clear conductance peaks. We perform conductance measurements of **1** and **1H** under 250 mV, 650 mV, and 850 mV bias voltages (for comparing 1D histograms of **1** with the addition of increasing amounts of TFA, see Figure S3). Based on the cyclic voltammetry measurement of **1** (Figure S4), the molecule has an electrochemical HOMO–LUMO gap of ∼0.87 eV, which is comparable to the large bias voltage of 850 mV. We are not certain if the high bias is beyond the oxidation potential of the molecule and hypothesize that, based on the conductance data, the molecule likely does not undergo oxidation reactions under these applied bias voltages.

We first focus on the conductance distributions of **1** and **1H** under different applied bias voltages. We find that, under a high bias voltage of 850 mV, the conductance peak becomes broader. To analyze this effect, we compile individual conductance-displacement traces into two-dimensional (2D) histograms, as shown in Figure 2e,f (a summary of all 2D histograms is provided in Figure S5). We find that both **1** and **1H** show a similar junction elongation length under all measured bias voltages (Table S1), indicating that protonation does not substantially affect the dynamics of the junction evolution during tip withdrawal. From most of the measured 2D histograms, we observe a sloped conductance plateau with a shoulder around 10^{-2} G_0, which contributes to the broad 1D conductance peak. We hypothesize that the broad conductance distributions are a result of the conductance variations from junction to junction, primarily due to the variations in the molecular junction conformations and binding geometries.

Next, we compare the conductance peak values of **1** and **1H**, which are plotted against the applied tip bias voltage in Figure 2g. We see that, under the 250 mV bias voltage, **1** and **1H** show similar conductance. Under higher bias voltages of 650 mV

and 850 mV, we observe a general trend of a larger junction conductance of **1H** compared to that of **1**. The largest increase in conductance is observed under 850 mV when a conductance value for **1H** under a molar ratio between **1** and TFA of 1:40 was measured to be four times that measured for **1** in the absence of TFA (Table S1). We do not observe a systematic conductance increase with an increasing amount of acid in the molecular solution and suspect that the TFA being volatile (boiling point 72.4 °C) and the evaporation of TFA and TCB (boiling point 214.4 °C) over the course of the measurement affects the amount of the protonated **1H**, thus affecting the measured single-molecule conductance. Indeed, when we compile 1D conductance histograms of the initial 1−1000 traces and the final 9001−10000 traces in one measurement, we see a conductance decrease with time, more prominent for molecular solutions with a molar ratio between **1** and TFA of 1:80 and 1:200 under 850 mV than that for the 1:40 case under the same bias voltage (Figure S6). We additionally see that this conductance shift resulting from likely the evaporation of the acid during one experiment is more significant than variations in conductance from experiments performed on different days (Figure S7).

We find that, as protonation attenuates the electron negativity of the nitrogen and enhances the electron deficiency of the diazapentalene ring, increased charge transport across the molecular wire occurs. The appearance of the absorption peak at a red-shifted position of 767 nm upon protonation corresponds to a smaller optical HOMO−LUMO gap, indicating a possible higher molecular conductance. To further investigate the different transport characteristics of **1** and **1H**, we next turn to density functional theory (DFT)-based calculations. Assuming coherent electron tunneling across these molecular junctions under zero temperature, the current is expressed as the following in the Landauer model,[31]

$$I = \frac{2e}{h} \int_{-eV/2}^{eV/2} T(E)\, \mathrm{d}E$$

where e is the magnitude of the electric charge carried by a single electron, h is the Planck constant, V is the applied bias voltage, and $T(E)$ is the energy-dependent transmission function.

Figure 3 presents the calculated transmissions T as a function of energy for the **1** (top) and **1H** (bottom) junctions.
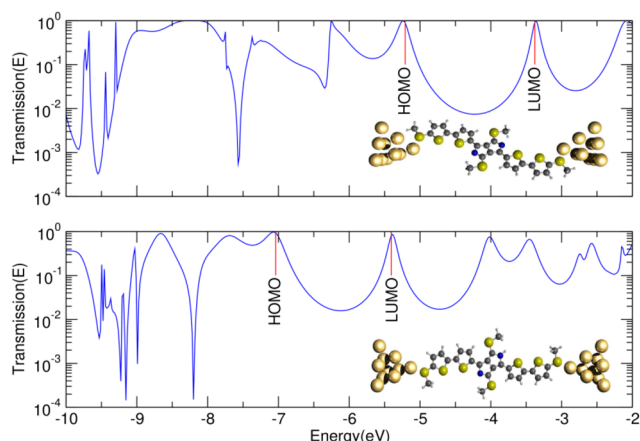

Figure 3. Transmissions for a single-molecule junction formed with deprotonated **1** (top) and protonated **1H** (bottom).

T can be roughly understood as the tunneling probability of an electron with a certain energy.[32] The first noticeable feature is the downward energy shift in the protonated form **1H**, resulting from the downward shift in MO energies due to the positive charge. This shift is largely an artifact of our computational setup, in which the electrodes are modeled as small finite gold clusters (with a constant density of states added in the transport calculation; see Supporting Information). In a realistic junction scenario, the positive charge would be at least partially screened, so it appears likely that, for both **1** and **1H**, the Fermi energy is somewhere between the HOMO and the LUMO. What we consider robust features of our simulations are (1) the broadening of the HOMO and LUMO peaks in the transmission upon protonation (the HOMO level broadened by 0.09 eV and LUMO level broadened by 0.05 eV; details can be found in the SI section IV) and (2) the peaks moving slightly closer together (in the unprotonated case, the HOMO−LUMO gap for the molecule in the junction, as evaluated from the central subsystem MOs, is 1.83 eV, and after protonation, the gap becomes 1.64 eV), both resulting in a larger transmission in the energy range between them.

Provided the dominant mechanism for electron transport is coherent tunneling, which is likely for short molecules as studied here, the zero-bias conductance can be estimated from T as $G(0V) = G_0 T(E_F)$.[32] As a first shot at $T(E_F)$, the minimum of T between the two peaks is around 0.7×10^{-2} for **1** and around 1.5×10^{-2} for **1H**, which would correspond to zero-bias conductances of $0.7 \times 10^{-2}\ G_0$ and $1.5 \times 10^{-2}\ G_0$, respectively. This agrees well with the experimentally observed increase in conductance upon protonation. At first sight, this would also agree quantitatively with the experimentally observed most likely conductance value for **1**. Note, however, that the Fermi energy E_F is notoriously difficult to predict from DFT calculations, as it depends on many factors such as the

detailed atomistic structure of the electrodes, solvent, or further adsorbed molecules in addition to the bridging one.[33,34] A value between around −5 eV and −4 eV would appear reasonable. This implies that the Fermi energy could be actually closer to the HOMO rather than in the middle of the two peaks, consistent with observations of hole transport being dominant in many conjugated hydrocarbons.[35] While this would not change our qualitative conclusions on the increase of conductance upon protonation, it would result in a higher simulated conductance. Rather than suggesting a mismatch between theory and simulations, this is in line with the known tendency of DFT to overestimate conductance by about an order of magnitude,[36−39] thus suggesting that our atomistic structures are a good representation of the structures responsible for the measured most likely conductances.

The broadening of the transmission peaks and their movement closer together is mirrored by the frontier molecular orbitals for the isolated molecules (Figure 4):
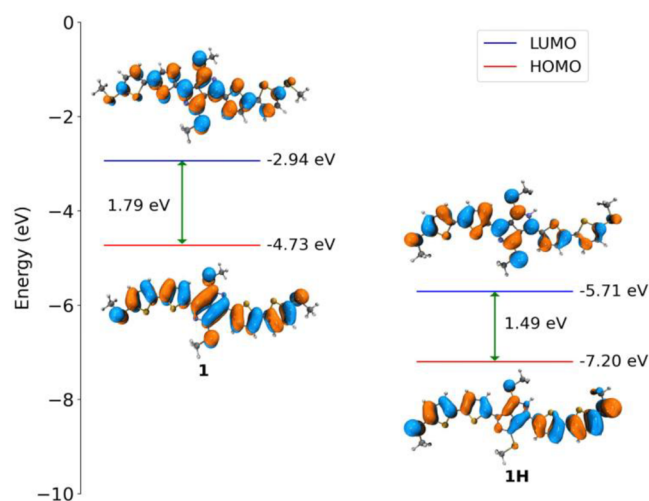

Figure 4. Energy level diagrams for HOMO and LUMO in both deprotonated **1** (left) and protonated **1H** (right) molecules.

Upon protonation, the MO coefficients at the anchoring groups increase, leading to larger electronic coupling to the electrodes, while at the same time, the energy gap between them decreases. Both effects favor larger transmissions and, therefore, higher conductances, in line with the experimental observations. This suggests that an inspection of frontier molecular orbitals for the isolated molecules can help predict conductance trends upon protonation, at least for cases where the effect of charging does not play a dominant role.

To summarize, we present a quantitative comparison of the single molecule charge transport properties of a diazapentalene compound in deprotonated and protonated state. The formation of diazapentalene single molecule junctions is enabled by the synthetic means to functionalize the diazapentalene with thiophene units and aurophilic contact groups. We find that addition of organic acid such as trifluoroacetic acid into a nonpolar solvent environment can successfully protonate the diazapentalene compound, providing an easy access to protonation without the requirement of an ionic solution and the use of a wax-coated tip. DFT calculations suggest that the higher conductance observed for the protonated molecule in comparison to the deprotonated one under high bias is a result of both broadened HOMO and

LUMO peaks and a reduced HOMO−LUMO gap. The lone pair electrons on the nitrogen in diazapentalene, similar to those in pyridine, are in the same plane as the ring; both diazapentalene and pyridine show a pH-regulated single molecule conductance.[13] We expect a lot to be learned about the pH-mediated modulation of single-molecule conductance in other nitrogen-containing cyclic systems in the future. The molecular material reported herein contributes to the continued development of novel molecular designs for the effective regulation of molecular conductance.

■ ASSOCIATED CONTENT

ⓢ Supporting Information

The Supporting Information is available free of charge at https://pubs.acs.org/doi/10.1021/acs.jpclett.4c02203.

> Experimental procedures, additional figures, and computational details (PDF)

■ AUTHOR INFORMATION

Corresponding Authors

Di Wu − *School of Chemistry, Chemical Engineering and Life Science, State Key Laboratory of Advanced Technology for Materials Synthesis and Processing, Center of Smart Materials and Devices, Wuhan University of Technology, Wuhan 430070, China;* ⓞ orcid.org/0000-0002-6721-739X; Email: chemwd@whut.edu.cn

Jianlong Xia − *State Key Laboratory of Advanced Technology for Materials Synthesis and Processing, Center of Smart Materials and Devices and School of Chemistry, Chemical Engineering and Life Science and International School of Materials Science and Engineering, Wuhan University of Technology, Wuhan 430070, China;* ⓞ orcid.org/0000-0003-2714-0786; Email: jlxia@whut.edu.cn

Haixing Li − *Department of Physics, City University of Hong Kong, Kowloon 999077, Hong Kong, China;* ⓞ orcid.org/0000-0002-1383-4907; Email: haixinli@cityu.edu.hk

Authors

Jianming An − *Department of Physics, City University of Hong Kong, Kowloon 999077, Hong Kong, China*

Xiaoqi Luo − *International School of Materials Science and Engineering and State Key Laboratory of Advanced Technology for Materials Synthesis and Processing, Center of Smart Materials and Devices and School of Chemistry, Chemical Engineering and Life Science, Wuhan University of Technology, Wuhan 430070, China*

Sumit Naskar − *Department of Chemistry, University of Hamburg, 22761 Hamburg, Germany; The Hamburg Centre for Ultrafast Imaging, University of Hamburg, 22761 Hamburg, Germany*

Carmen Herrmann − *Department of Chemistry, University of Hamburg, 22761 Hamburg, Germany; The Hamburg Centre for Ultrafast Imaging, University of Hamburg, 22761 Hamburg, Germany*

Complete contact information is available at:
https://pubs.acs.org/10.1021/acs.jpclett.4c02203

Author Contributions

○J.A. and X.L. contributed equally.

Notes

The authors declare no competing financial interest.

■ REFERENCES

(1) Wu, B.; Guo, W.; An, J.; Li, H. Control of molecular conductance by pH. *Journal of Materials Chemistry C* **2022**, *10* (37), 13483−13498.

(2) Stone, I.; Starr, R. L.; Zang, Y.; Nuckolls, C.; Steigerwald, M. L.; Lambert, T. H.; Roy, X.; Venkataraman, L. A single-molecule blueprint for synthesis. *Nature Reviews Chemistry* **2021**, *5* (10), 695−710.

(3) Chen, F.; Li, X. L.; Hihath, J.; Huang, Z. F.; Tao, N. J. Effect of anchoring groups on single-molecule conductance: Comparative study of thiol-, amine-, and carboxylic-acid-terminated molecules. *J. Am. Chem. Soc.* **2006**, *128* (49), 15874−15881.

(4) Ahn, S.; Aradhya, S. V.; Klausen, R. S.; Capozzi, B.; Roy, X.; Steigerwald, M. L.; Nuckolls, C.; Venkataraman, L. Electronic transport and mechanical stability of carboxyl linked single-molecule junctions. *Physical chemistry chemical physics: PCCP* **2012**, *14* (40), 13841−5.

(5) Lawson, B.; Skipper, H. E.; Kamenetska, M. Phenol is a pH-activated linker to gold: a single molecule conductance study. *Nanoscale* **2024**, *16* (4), 2022−2029.

(6) Pan, X. Y.; Lawson, B.; Rustad, A. M.; Kamenetska, M. pH-Activated Single Molecule Conductance and Binding Mechanism of Imidazole on Gold. *Nano Lett.* **2020**, *20* (6), 4687−4692.

(7) Wu, C. L.; Alqahtani, A.; Sangtarash, S.; Vezzoli, A.; Sadeghi, H.; Robertson, C. M.; Cai, C. X.; Lambert, C. J.; Higgins, S. J.; Nichols, R. J. In situ formation of H-bonding imidazole chains in break-junction experiments. *Nanoscale* **2020**, *12* (14), 7914−7920.

(8) Herrer, I. L.; Ismael, A. K.; Milan, D. C.; Vezzoli, A.; Martin, S.; Gonzalez-Orive, A.; Grace, I.; Lambert, C.; Serrano, J. L.; Nichols, R. J.; Cea, P. Unconventional Single-Molecule Conductance Behavior for a New Heterocyclic Anchoring Group: Pyrazolyl. *J. Phys. Chem. Lett.* **2018**, *9* (18), 5364−5372.

(9) Herrer, L.; Martin, S.; Gonzalez-Orive, A.; Milan, D. C.; Vezzoli, A.; Nichols, R. J.; Serrano, J. L.; Cea, P. pH control of conductance in a pyrazolyl Langmuir-Blodgett monolayer. *J. Mater. Chem. C* **2021**, *9* (8), 2882−2889.

(10) Zhang, Y.-P.; Chen, L.-C.; Zhang, Z.-Q.; Cao, J.-J.; Tang, C.; Liu, J.; Duan, L.-L.; Huo, Y.; Shao, X.; Hong, W.; Zhang, H.-L. Distinguishing Diketopyrrolopyrrole Isomers in Single-Molecule Junctions via Reversible Stimuli-Responsive Quantum Interference. *J. Am. Chem. Soc.* **2018**, *140* (21), 6531−6535.

(11) Tang, C.; Huang, L.; Sangtarash, S.; Noori, M.; Sadeghi, H.; Xia, H.; Hong, W. Reversible Switching between Destructive and Constructive Quantum Interference Using Atomically Precise Chemical Gating of Single-Molecule Junctions. *J. Am. Chem. Soc.* **2021**, *143* (25), 9385−9392.

(12) Baghernejad, M.; Manrique, D. Z.; Li, C.; Pope, T.; Zhumaev, U.; Pobelov, I.; Moreno-Garcia, P.; Kaliginedi, V.; Huang, C.; Hong, W.; Lambert, C.; Wandlowski, T. Highly-effective gating of single-molecule junctions: an electrochemical approach. *Chem. Commun. (Camb)* **2014**, *50* (100), 15975−8.

(13) Brooke, R. J.; Szumski, D. S.; Vezzoli, A.; Higgins, S. J.; Nichols, R. J.; Schwarzacher, W. Dual Control of Molecular Conductance through pH and Potential in Single-Molecule Devices. *Nano Lett.* **2018**, *18* (2), 1317−1322.

(14) Morales, G. M.; Jiang, P.; Yuan, S. W.; Lee, Y. G.; Sanchez, A.; You, W.; Yu, L. P. Inversion of the rectifying effect in diblock molecular diodes by protonation. *J. Am. Chem. Soc.* **2005**, *127* (30), 10456−10457.

(15) Darwish, N.; Aragonès, A. C.; Darwish, T.; Ciampi, S.; Díez-Pérez, I. Multi-Responsive Photo- and Chemo-Electrical Single-Molecule Switches. *Nano Lett.* **2014**, *14* (12), 7064−7070.

(16) Kumar, S.; Merelli, M.; Danowski, W.; Rudolf, P.; Feringa, B. L.; Chiechi, R. C. Chemical Locking in Molecular Tunneling Junctions Enables Nonvolatile Memory with Large On-Off Ratios. *Adv. Mater.* **2019**, *31* (15), No. e1807831.

(17) Yang, G.; Sangtarash, S.; Liu, Z.; Li, X.; Sadeghi, H.; Tan, Z.; Li, R.; Zheng, J.; Dong, X.; Liu, J.; Yang, Y.; Shi, J.; Xiao, Z.; Zhang, G.; Lambert, C.; Hong, W.; Zhang, D. Protonation tuning of quantum interference in azulene-type single-molecule junctions. *Chem. Sci.* **2017**, *8* (11), 7505−7509.

(18) Cai, S.; Deng, W.; Huang, F.; Chen, L.; Tang, C.; He, W.; Long, S.; Li, R.; Tan, Z.; Liu, J.; Shi, J.; Liu, Z.; Xiao, Z.; Zhang, D.; Hong, W. Light-Driven Reversible Intermolecular Proton Transfer at Single-Molecule Junctions. *Angew. Chem., Int. Ed.* **2019**, *58* (12), 3829−3833.

(19) Xiao, X. Y.; Xu, B. Q.; Tao, N. J. Conductance titration of single-peptide molecules. *J. AM. Chem. Soc.* **2004**, *126* (17), 5370−5371.

(20) Brisendine, J. M.; Refaely-Abramson, S.; Liu, Z.-F.; Cui, J.; Ng, F.; Neaton, J. B.; Koder, R. L.; Venkataraman, L. Probing Charge Transport through Peptide Bonds. *J. Phys. Chem. Lett.* **2018**, *9* (4), 763−767.

(21) Scullion, L.; Doneux, T.; Bouffier, L.; Fernig, D. G.; Higgins, S. J.; Bethell, D.; Nichols, R. J. Large Conductance Changes in Peptide Single Molecule Junctions Controlled by pH. *J. Phys. Chem. C* **2011**, *115* (16), 8361−8368.

(22) Li, Z.; Smeu, M.; Afsari, S.; Xing, Y.; Ratner, M. A.; Borguet, E. Single-molecule sensing of environmental pH–an STM break junction and NEGF-DFT approach. *Angew. Chem., Int. Ed.* **2014**, *53* (4), 1098−102.

(23) Ai, Q. S.; Fu, Q.; Liang, F. pH-Mediated Single Molecule Conductance of Cucurbit[7]uril. *Front. Chem.* **2020**, *8*, 1.

(24) Qian, G.; Wang, Z. Y. Near-Infrared Thermochromic Diazapentalene Dyes. *Adv. Mater.* **2012**, *24* (12), 1582−1588.

(25) Dell, E. J.; Capozzi, B.; Xia, J.; Venkataraman, L.; Campos, L. M. Molecular length dictates the nature of charge carriers in single-molecule junctions of oxidized oligothiophenes. *Nat. Chem.* **2015**, *7* (3), 209−214.

(26) Khelifi, W.; Awada, H.; Brymora, K.; Blanc, S.; Hirsch, L.; Castet, F.; Bousquet, A.; Lartigau-Dagron, C. Halochromic Switch from the 1st to 2nd Near-Infrared Window of Diazapentalene−Dithienosilole Copolymers. *Macromolecules* **2019**, *52* (13), 4820−4827.

(27) Qian, G.; Qi, J.; Davey, J. A.; Wright, J. S.; Wang, Z. Y. Family of Diazapentalene Chromophores and Narrow-Band-Gap Polymers: Synthesis, Halochromism, Halofluorism, and Visible−Near Infrared Photodetectivity. *Chem. Mater.* **2012**, *24* (12), 2364−2372.

(28) Xu, B.; Tao, N. J. Measurement of Single-Molecule Resistance by Repeated Formation of Molecular Junctions. *Science* **2003**, *301* (5637), 1221−1223.

(29) Venkataraman, L.; Klare, J. E.; Tam, I. W.; Nuckolls, C.; Hybertsen, M. S.; Steigerwald, M. L. Single-Molecule Circuits with Well-Defined Molecular Conductance. *Nano Lett.* **2006**, *6* (3), 458−462.

(30) Guo, W.; Quainoo, T.; Liu, Z.-F.; Li, H. Robust binding between secondary amines and Au electrodes. *Chem. Commun.* **2024**, *60*, 3393.

(31) Datta, S. *Electronic transport in mesoscopic systems*; Cambridge University Press, 1997.

(32) Scheer, E.; Cuevas, J. C. *Molecular electronics: an introduction to theory and experiment*; World Scientific, 2017; Vol. *15*.

(33) Draxl, C.; Nabok, D.; Hannewald, K. Organic/Inorganic Hybrid Materials: Challenges for ab Initio Methodology. *Acc. Chem. Res.* **2014**, *47* (11), 3225−3232.

(34) Egger, D. A.; Liu, Z.-F.; Neaton, J. B.; Kronik, L. Reliable Energy Level Alignment at Physisorbed Molecule−Metal Interfaces from Density Functional Theory. *Nano Lett.* **2015**, *15* (4), 2448−2455.

(35) Park, S.; Kang, H.; Yoon, H. J. Structure−thermopower relationships in molecular thermoelectrics. *Journal of Materials Chemistry A* **2019**, *7* (24), 14419−14446.

(36) Feng, Q.; Yamada, A.; Baer, R.; Dunietz, B. D. Deleterious Effects of Exact Exchange Functionals on Predictions of Molecular Conductance. *J. Chem. Theory Comput.* **2016**, *12* (8), 3431−3435.

(37) Strange, M.; Rostgaard, C.; Hakkinen, H.; Thygesen, K. S. Self-consistent GW calculations of electronic transport in thiol- and amine-linked molecular junctions. *Phys. Rev. B* **2011**, *83* (11), No. 115108.

(38) Koentopp, M.; Chang, C.; Burke, K.; Car, R. Density functional calculations of nanoscale conductance. *J. Phys.: Condens. Matter* **2008**, *20* (8), No. 083203.

(39) Ke, S. H.; Baranger, H. U.; Yang, W. Role of the exchange-correlation potential in ab initio electron transport calculations. *J. Chem. Phys.* **2007**, *126* (20), No. 201102.